Received: 8 March 2022 | Revised: 31 May 2022 | Accepted: 24 June 2022

DOI: 10.1002/pro.4385

FULL-LENGTH PAPER

Ca^{2+}-dependent interactions between lipids and the tumor-targeting peptide pHLIP

Victor Vasquez-Montes[1] | **Vivek Tyagi**[2] | **Eden Sikorski**[3] | **Alexander Kyrychenko**[4] | **J. Alfredo Freites**[2] | **Damien Thévenin**[3] | **Douglas J. Tobias**[2] | **Alexey S. Ladokhin**[1]

[1]Department of Biochemistry and Molecular Biology, The University of Kansas Medical Center, Kansas City, Kansas, USA

[2]Department of Chemistry, University of California, Irvine, California, USA

[3]Department of Chemistry, Lehigh University, Bethlehem, Pennsylvania, USA

[4]Institute of Chemistry and School of Chemistry, V. N. Karazin Kharkiv National University, Kharkiv, Ukraine

Correspondence
Damien Thévenin, Department of Chemistry, Lehigh University, Bethlehem, PA 18015, USA.
Email: dat311@lehigh.edu

Douglas J. Tobias, Department of Chemistry, University of California, Irvine, CA 92697, USA.
Email: douglas.tobias@uci.edu

Alexey S. Ladokhin, Department of Biochemistry and Molecular Biology, The University of Kansas Medical Center, Kansas City, KS 66160, USA.
Email: aladokhin@kumc.edu

Funding information
NIH Clinical Center, Grant/Award Numbers: R01 GM116961, R01 GM126778; KUMC

Review Editor: Nir Ben-Tal

Abstract

Cancerous tissues undergo extensive changes to their cellular environments that differentiate them from healthy tissues. These changes include changes in extracellular pH and Ca^{2+} concentrations, and the exposure of phosphatidylserine (PS) to the extracellular environment, which can modulate the interaction of peptides and proteins with the plasma membrane. Deciphering the molecular mechanisms of such interactions is critical for advancing the knowledge-based design of cancer-targeting molecular tools, such as pH-low insertion peptide (pHLIP). Here, we explore the effects of PS, Ca^{2+}, and peptide protonation state on the interactions of pHLIP with lipid membranes. Cellular studies demonstrate that exposed PS on the plasma membrane promotes pHLIP targeting. The magnitude of this effect is dependent on extracellular Ca^{2+} concentration, indicating that divalent cations play an important role in pHLIP targeting in vivo. The targeting mechanism is further explored with a combination of fluorescence and circular dichroism experiments in model membranes and microsecond-timescale all-atom molecular dynamics simulations. Our results demonstrate that Ca^{2+} is engaged in coupling peptide-lipid interactions in the unprotonated transmembrane conformation of pHLIP. The simulations reveal that while the pH-induced insertion leads to a strong depletion of PS around pHLIP, the Ca^{2+}-induced insertion has the opposite effect. Thus, extracellular levels of Ca^{2+} are crucial to linking cellular changes in membrane lipid composition with the selective targeting and insertion of pHLIP. The characterized Ca^{2+}-dependent coupling between pHLIP sidechains and PS provides atomistic insights into the general mechanism for lipid-coupled regulation of protein-membrane insertion by divalent cations.

KEYWORDS
lipid bilayer, membrane protein, molecular dynamics, protein-lipid interaction, spectroscopy, tumor therapy

Victor Vasquez-Montes, Vivek Tyagi, and Eden Sikorski contributed equally to this work.

1 | INTRODUCTION

Characteristic differences in pH, ionic, and charged macromolecule concentrations between tissues, cells, and organelles can trigger functionally relevant structural rearrangements in protein systems transitioning between different environments. The conformational switching associated with the water-to-membrane partitioning of membrane-active peptides and proteins constitutes a prominent example of such transitions. Proteins in this group include bacterial toxins,[1,2] viral entry proteins,[3] antimicrobial peptides,[4] cancer-targeting peptides,[5–7] and Bcl-2 apoptotic regulators.[8,9] Their significant involvement in human disease and treatment makes them fundamentally important to the biomedical field and the focus of many studies. Unfortunately, our knowledge of the basic mechanism of conformational switching in membrane systems is often lacking, impeding our ability to predict protein-lipid interactions and the resulting conformations under physiological conditions. Specifically, the role of lipid composition and divalent cations in modulating these interactions remains under-explored, despite the mounting evidence of their physiological importance in triggering (together with $[H^+]$ differences) functionally relevant conformational changes.[9–16] Our ability to target or manipulate these processes can therefore be beneficial for human health.

A prominent example of the interplay between pH, lipid composition, and divalent cation modulation on peptide/membrane interaction is the regulation of the tumor-targeting peptide pH-low insertion peptide (pHLIP).[17] A peptide system that has recently been used to target drugs to cancer cells.[5,6,18–20] The selective targeting of pHLIP to cancerous tissues has been traditionally attributed to the mildly acidic extracellular environment generated by these tissues.[21,22] Physiological levels of divalent cations[17] and differences in membrane lipids[23–26] have been demonstrated to also be involved in the targeting and insertion propensities of pHLIP. While the constant presence of the former in plasma is expected to be a persistent modulator, differences in lipid composition between healthy and cancer cells are hypothesized to affect pHLIP's selectivity. A particular emphasis has been placed on the anionic lipid phosphatidylserine (PS).[17,23–25] This is due to the characteristic loss of lipid asymmetry in the plasma membranes of cancer cells that leads to the exposure of the anionic lipid PS.[11–13] While the level of exposed PS in the outer leaflet varies between cancer cell lines,[11,12,27–29] and by extension also the remaining PS fraction in the inner leaflet, PS exposure grants cancerous cells an anionic extracellular surface that differentiates them from the zwitterionic surface of healthy cells.[11,30] However, the impact of exposed PS on the interaction of peptides/proteins with cancer cells remains unclear.

In the case of pHLIP, our recent publications demonstrate that its selective targeting and insertion mechanism involves intimate coupling between pH, extracellular divalent cations, and membrane lipid composition.[17,23,24]

Here, we expand on these results and investigate the intricate relationship between PS lipids and physiological levels of divalent cations on the tumor targeting and selectivity properties of pHLIP. To this end, we performed a series of cellular and biophysical studies in combination with microsecond timescale all-atom molecular dynamics (MD) simulations. Our results show that the presence of Ca^{2+} is crucial to linking the effects of elevated PS levels in cancer cells to the cellular targeting of pHLIP. MD simulations revealed extensive Ca^{2+}-mediated interactions between pHLIP acidic sidechains and membrane lipids that stabilize the unprotonated transmembrane form of pHLIP. They also demonstrate that the pH- and Ca^{2+}-driven insertion produces different local distributions of PS lipids around pHLIP. These results highlight the significance of divalent cations on protein-membrane interactions and show that they must be considered to understand peptide-membrane interactions in biological settings and the design of membrane-interacting peptides.

2 | RESULTS

2.1 | Ca^{2+} enhances the effects of PS on pHLIP cellular targeting

The effect of extracellularly exposed PS on pHLIP cellular targeting was measured by flow cytometry using a fluorescently labeled pHLIP conjugate. Measurements were performed on two cell lines with different levels of exposed PS, as confirmed by Annexin V binding (Figure S1): LNCap cells (high PS) exhibit twice as much PS at their surface than HEK293 cells (low PS), a fold difference consistent with what has been observed between cancerous and noncancerous cell lines.[11,12,31]

At physiological pH 7.4, AlexaFluor488-tagged pHLIP showed minor interactions with cells in the absence of divalent cations, consistent with previously published results[17] (Figure 1). This interaction was, however, enhanced either by the presence of 1.8 mM Ca^{2+} (mimicking total extracellular [divalent cation]) at pH 7.4 or mild acidification to pH 7.0 (resembling tumor tissue pH[21,22]). The former results in a 3.2-fold increase in pHLIP cellular interactions, while a 1.6-fold increase was observed for the latter regardless of $[Ca^{2+}]$. The Ca^{2+}-induced increase in pHLIP cellular interactions in both

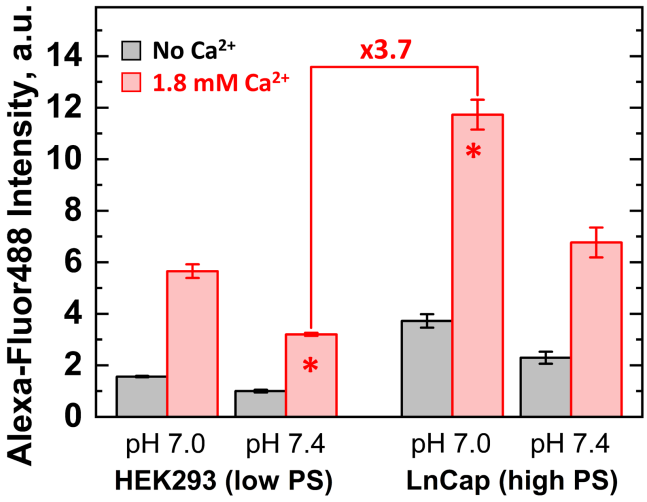

FIGURE 1 Modulation of the cellular targeting of pH-low insertion peptide (pHLIP) by phosphatidylserine (PS) and Ca^{2+}. Flow cytometry measurements of pHLIP N-terminally conjugated to AlexaFluor-488 in cell lines with different levels of exposed plasma membrane PS. Differences in outer leaflet PS levels were determined by Annexin V (Figure S1). Mild acidification alone (in the absence of Ca^{2+}) resulted in an average 1.6-fold increase in pHLIP cellular interactions, while the addition of 1.8 mM Ca^{2+} at pH 7.4 led to a 3.2-fold increase. The substantial increase observed in the presence of Ca^{2+} (red) points to its significant role in the cellular targeting of pHLIP at the pH range produced by tumors. These effects were further enhanced by larger levels of exposed PS in the plasma membrane. A 3.7-fold increase in pHLIP cellular interactions (indicated by the asterisks) was observed under conditions that recapitulate cellular differentiation at 1.8 mM Ca^{2+} to represent extracellular divalent cation levels. "Healthier cells": Low PS at pH 7.4, "cancerous cells": High PS at pH 7.0

cell lines, irrespective of pH, is consistent with its delivery capabilities into MDA-MB-231 cancer cells in the presence of Ca^{2+},[17] confirming the importance of divalent cations on pHLIP cellular targeting.

The magnitude of the Ca^{2+}-dependent and pH-dependent effects are modulated by the content of extracellularly exposed PS at the plasma membrane. Higher levels of exposed PS in LNCap cells resulted in significantly higher pHLIP targeting compared to HEK293 cells (Figure 1). Notably, the twofold increase in pHLIP targeting observed between the two cell lines correlates with the twofold difference in the relative level of PS exposure. This is particularly the case in the presence of Ca^{2+} (Figure 1, red), as exemplified by the data indicated by asterisks, which represents changes in cellular conditions during tumor progression: from "healthier tissue" (low PS at pH 7.4) to "cancerous tissue" (high PS at pH 7.0), where a 3.7-fold difference in fluorescent signal was observed between these two conditions in the presence of Ca^{2+}.

These results show that changes in the levels of extracellularly exposed PS in the plasma membrane of tumor cells have a substantial role in the cellular targeting of pHLIP and are likely key to its selectivity. The enhanced targeting of PS-rich cells, however, requires the presence of extracellular levels of divalent cations, as their absence in our "cancerous" model (high PS at pH 7.0) only reached 32% of the maximal signal determined in the presence of Ca^{2+}. The effect of exposed PS plus divalent cations on the selectivity of tumor vs. healthy cells is expected to be larger in vivo due to the lack of exposed PS in healthy cells[11–13,30] (unlike our "healthier" model cells which come from a differentiated cell line with measurable levels of exposed PS).

2.2 | Low pH and Ca^{2+} induce the same transmembrane state of pHLIP

The combined effects of Ca^{2+} and pH on the bilayer insertion of pHLIP were further analyzed in vitro using a combination of spectroscopic measurements and MD simulations. The membranes contained a 3:1 M mixture of zwitterionic phosphatidylcholine (POPC) and anionic phosphatidylserine (POPS).

The transmembrane insertion of pHLIP into large unilamellar vesicles (LUV) was determined using Trp fluorescence, taking advantage of its two native Trp residues. The extensive use of Trp fluorescence in pHLIP studies provides well-established benchmarks for its two membrane-associated states (interfacial and transmembrane) in different lipid compositions.[23–26,32] In the case of POPS-containing membranes, the interfacial form of pHLIP is characterized by a Trp λ_{Max} ~357 nm, while its transmembrane form has a Trp λ_{Max} ~343 nm.[23,24] In the absence of divalent cations, the addition of 3:1 POPC:POPS LUVs at pH 10 produced a Trp λ_{Max} ~356 nm, consistent with its interfacial state (Figure 2a, green). The gradual increase in Ca^{2+} at this pH, however, led to significant decreases in fluorescence maximum values until saturation was achieved at 3 mM Ca^{2+}, where a Trp λ_{Max} ~343 nm, characteristic of pHLIP's transmembrane state, was obtained (Figure 2a, orange). Acidification to pH 4.5 in the absence of Ca^{2+} produced an equivalent Trp λ_{Max} as the one determined at pH 10 and 3 mM Ca^{2+}. The equivalent Trp λ_{Max} obtained by acidification or Ca^{2+} indicates that both conditions produce pHLIP conformations in the bilayer that place the Trp sidechains in similar environments.

The presence of Ca^{2+} had the added effect of shifting the pH-dependent insertion of pHLIP toward

physiological pH ranges. For example, at 1 mM Ca^{2+} pHLIP presents a pK_{50} of 7.3 (Figure 2a, cyan), corresponding to a 2-pH unit shift compared to the pK_{50} observed in the absence of Ca^{2+} (Figure 2a, green) and has a near complete insertion at ~pH 6. In contrast, 2 mM Ca^{2+} led to the complete insertion of pHLIP at pH 7.2 in the same lipid composition with a $pK_{50} = 7.8$,[17] suggesting that slight changes in $[Ca^{2+}]$ can have drastic effects on the pH-dependent insertion of pHLIP.

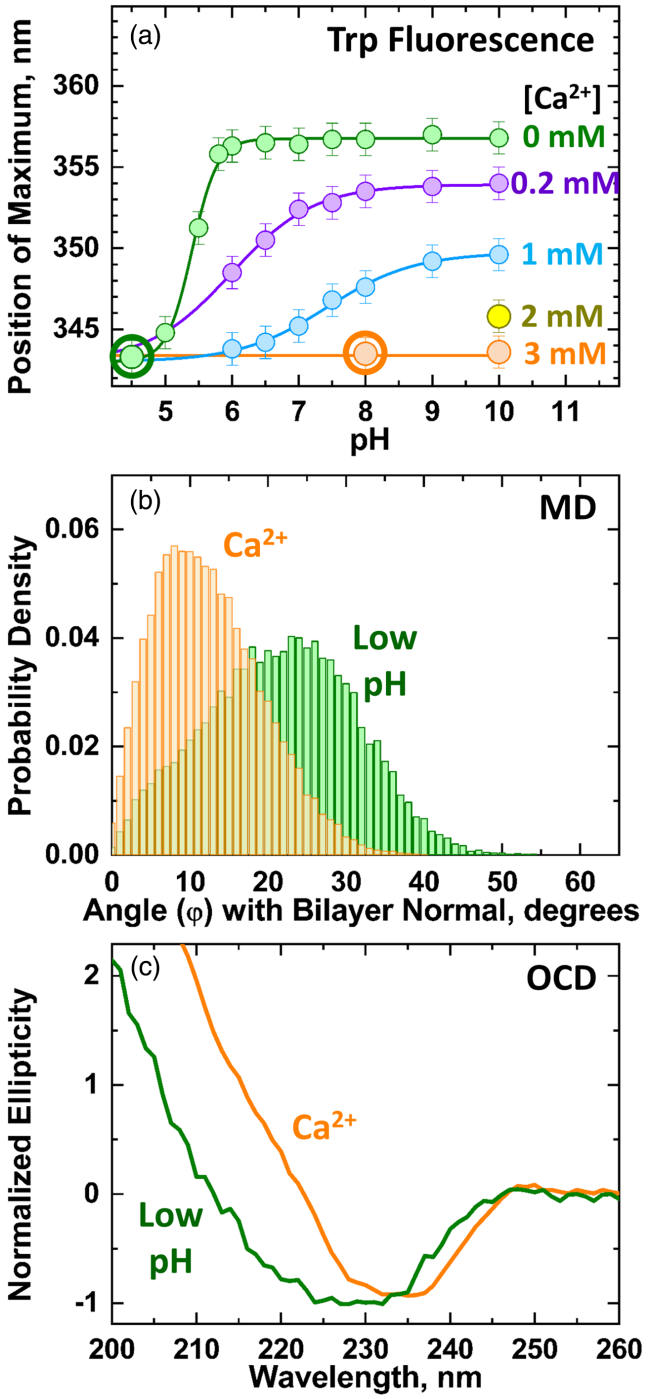

2.3 | Transverse position of pHLIP at low pH and in the presence of Ca^{2+}

To study the role of divalent cations on the interactions of pHLIP with lipids, we performed two microsecond timescale all-atom MD simulations of pHLIP embedded in a 3:1 POPC:POPS lipid bilayer: a "low pH" condition, where all pHLIP acidic residues are protonated; and a "Ca^{2+}" condition, where pHLIP is at neutral pH, modeled as a singly protonated aspartate residue (D25) in the presence of 0.1 M $CaCl_2$ (see Section 4). All acidic residues (except D25) were left unprotonated in the latter due to their interfacial positioning in constant-pH simulations of transmembrane pHLIP,[35] where they potentially serve as Ca^{2+}-coordinating moieties. Meanwhile, D25 (located near the middle of the bilayer) was set in a protonated state to reduce its thermodynamic penalty to insert into the bilayer.

First, we compared the topology of transmembrane pHLIP in both simulations using the tilt angles generated between the peptide helical axis and the lipid bilayer normal (Figure 2 and Figure S2). The corresponding distributions (Figure 2b) show that pHLIP in the presence of Ca^{2+} adopts a more perpendicular orientation (Figure 2b, orange) than the one observed under the low pH condition (Figure 2b, green). These results were confirmed by oriented circular dichroism spectroscopy (OCD), which allows the differentiation between transmembrane and interfacial α-helices.[33,34] OCD measurements at pH 8 in the presence of Ca^{2+} or low pH (pH 4, no Ca^{2+}) yielded

FIGURE 2 Protonation-dependent and independent insertion of pH-low insertion peptide (pHLIP) in anionic membranes (3:1 POPC:POPS). The transmembrane insertion of pHLIP is produced by acidity-induced protonation (green) or the presence of divalent cations (orange). (a) Transmembrane insertion of pHLIP at various $[Ca^{2+}]$ determined by Trp fluorescence. Extracellular levels of Ca^{2+} promote the pH-dependent insertion of pHLIP, resulting in a pK_{50} shift. Ca^{2+} also induces the protonation independent insertion of pHLIP. Large circles represent two conditions in which the rest of the measurements were performed: low pH (green); neutral pH with Ca^{2+} (orange). (b) Peptide tilt angles (φ) were calculated by measuring the deviation of the helix axis from the bilayer normal. Differences in width and peak position of the corresponding tilt angle distributions suggest that Ca^{2+} promotes a more stable orientation of the helix with small-angle deviations from the membrane normal. (c) Oriented circular dichroism spectra of pHLIP at low pH or in the presence of Ca^{2+}. Both conditions produced a single minimum at ~230 nm, confirming their transmembrane orientation.[33,34] The broadening of the low pH sample below 230 nm is consistent with a larger tilt relative to the bilayer normal.[33,34]

spectra with a single minimum around 230 nm (Figure 2c), consistent with transmembrane helices.[33,34] The spectrum measured at low pH, however, presented a broader minimum (Figure 2c, green) compared to the spectrum in the presence of Ca^{2+} (Figure 2c, orange). Given that measurements at low pH were conducted at pH 4, where pHLIP is in its inserted conformation,[36,37] the spectral broadening was attributed to a higher tilt angle as compared to the spectrum in the presence of Ca^{2+}, consistent with the MD simulations (Figure 2b).

The MD simulation results were further validated by the experimental determination of the depth of pHLIP penetration in the bilayer at low pH and in the presence of Ca^{2+}. The bilayer depth of W15 was used as a reference point to compare the insertion of pHLIP in the simulations and experiments. W15 represents one of the two native Trp in pHLIP and resides below the phosphate level in the transmembrane form of pHLIP induced by low pH.[38] Experimental determination of Trp depth was performed by depth-dependent quenching using brominated lipids,[39] which contain bromine atoms attached at various depths to the acyl chains.[40–42] (To ensure the selectivity, the other native W9 was replaced with Phe, which does not affect membrane interactions.[43])

Quenching measurements were performed using POPS-containing LUVs with a 50% molar ratio of brominated PC lipids. The resulting quenching data was compared to the unquenched sample ($F_0/F - 1$) and analyzed using the distribution-analysis (DA) methodology.[40–42] The bilayer penetration of the residues is reported as their distance from the bilayer center (Figure 3a,b). Results from depth-dependent quenching experiments were fitted using a double Gaussian distribution to account for the quenching from the trans-leaflet (Figure 3a,b). The resulting quenching profiles (QP) are used to determine the most probable depth (h_m) of the measured Trp,[40–42] which corresponded to 10.0 ± 1.2 Å and 9.1 ± 0.2 Å away from the bilayer center at low pH and in the presence of Ca^{2+}, respectively.

The distributions of W15 depths determined by the MD simulations were consistent with the quenching results (Figure 3) and captured the decrease in distribution widths in the presence of Ca^{2+}. All calculated parameters are summarized in Table S1.

Having validated the MD simulation trajectories with the comparison to spectroscopic measurements, we used the MD simulation results to generate insights into the role of Ca^{2+}-mediated interactions and pHLIP protonation in stabilizing pHLIP in a transmembrane configuration in PS-containing membranes. To further characterize the pHLIP configuration, we compared the bilayer distributions of all acidic residues (E3, D14, 25, D31, D33, and D34) in the low pH and Ca^{2+} simulations (Figure 3c,d). All residues were described by a single Gaussian distribution, except for E3 in the presence of Ca^{2+}, which was best described by a sum of two gaussian distributions. As in the case of W15 (Figure 3a, b), the distributions of all acidic residues in the Ca^{2+} simulation are narrower than those observed at low pH. This can be attributed to possible stabilizing effects of Ca^{2+}-mediated pHLIP-lipid interactions. Calculated depths and distribution widths are summarized in Table S1.

2.4 | Ca^{2+} mediates interactions between lipids and pHLIP

The pHLIP-Ca^{2+} and pHLIP-Ca^{2+}-lipid interactions were determined from the analysis of the Ca^{2+} first coordination shell in the corresponding radial distribution function between Ca^{2+}-moiety pairs indicated in Figure 4. All charged acidic residues in pHLIP interact with Ca^{2+}, predominantly without lipid participation (Figure 4a,b, gray). The most frequent interactions involve D14 and D31, both of which are located close to the lipid bilayer polar/apolar interface in either leaflet (Figure 3d). Charged acidic residues were also observed to interact with POPC and POPS lipids through Ca^{2+}-mediated interactions (Figure 4a,b, red; and Figure 4c). The largest number of pHLIP-Ca^{2+}-lipid interactions also involved the acidic residues D14 (top leaflet) and D31 (bottom leaflet), which account for 38 and 36% of all pHLIP-Ca^{2+}-lipid interactions, respectively (Figure S3).

The disproportionate number of interactions between D14/D31 and Ca^{2+} compared to shallower residues is likely due to the Ca^{2+}-driven stabilization of unprotonated aspartate and glutamate charges. These interactions would reduce the thermodynamic penalty of positioning charged groups in the membrane and are facilitated by the enrichment of Ca^{2+} near the phosphates and carbonyl oxygens in the bilayer.[44] Separating the Ca^{2+}-mediated lipid interactions of pHLIP (Figure 4a, b, red) by lipid species revealed that POPS is involved in 38% of all lipid interactions, despite only comprising 25% of the bilayer lipids, suggesting its enrichment around pHLIP in the presence of Ca^{2+}.

2.5 | Ca^{2+} modulates the PS environment around pHLIP

We then inspected the possible effect of Ca^{2+} on the lipid environment surrounding transmembrane pHLIP, as the content and asymmetry of PS in the bilayer are crucial modulators of pHLIP insertion.[23–25] The lipid environment in the MD simulations was characterized by

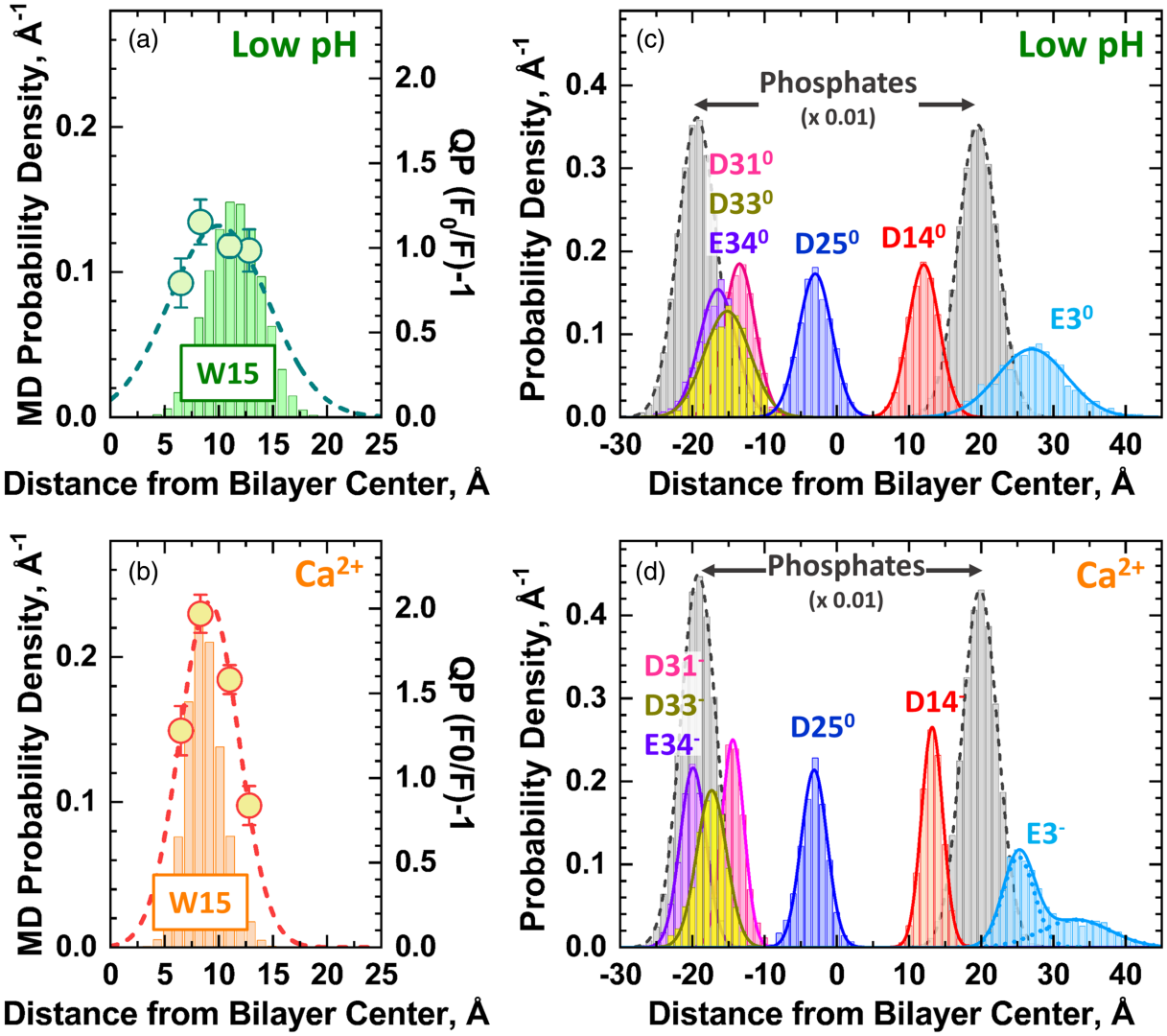

FIGURE 3 Transverse distributions of key residues in transmembrane pH-low insertion peptide (pHLIP). (a and b) Comparison between experimentally determined W15 bilayer depth penetration by bromolipid-quenching (circles) and its distribution in the bilayer determined by molecular dynamics (MD) (bars). The quenching profile (QP) of pHLIP-W15 (dashed line) indicates the most probable depth of the residue. The profile was obtained by fitting the data to a double gaussian distribution as described by the distribution analysis methodology.[41] Error bars indicate the average of two independent quenching measurements. The corresponding probability density histograms from the MD simulations (shown as bars) are consistent with the experimental results and recapitulate differences in depth and distribution width at (a) low pH (MD: all E and D protonated, QP: pH 4) and (b) in the presence of Ca^{2+} (MD: protonated D25, QP: 2 mM Ca^{2+} at pH 8). (c and d) The acidic residue distributions from the MD simulations yield equivalent positions for both low pH and Ca^{2+} conditions. The decrease in distribution width observed for W15 in the presence of Ca^{2+} is also observed in the acidic residues. All distribution profiles are well described by a single gaussian distribution, except for E3 in the presence of Ca^{2+}, which was better represented by a sum of two Gaussians. The corresponding distribution parameters are summarized in Table S1. Distributions of phosphates in each bilayer are shown in gray as a visual reference of the bilayer.

calculating the fraction of POPS lipids within a 15-Å radius of the peptide throughout the simulation (Figure 5). The top and bottom leaflets were treated separately, with the top leaflet helix center measured from the center of mass of residues 13 to 16. Similarly, the bottom leaflet helix center was measured from the center of mass of residues 27 to 32. The results were then compared to the nominal fraction of POPS lipids in the simulated bilayer (dashed lines in Figure 5). The time traces and corresponding probability densities for the POPS fraction show significant differences between the low pH and Ca^{2+} simulations, with the latter exhibiting larger POPS fractions in the vicinity of pHLIP in both leaflets.

To experimentally confirm the depletion of PS in the trans-leaflet observed in the MD simulation of protonated

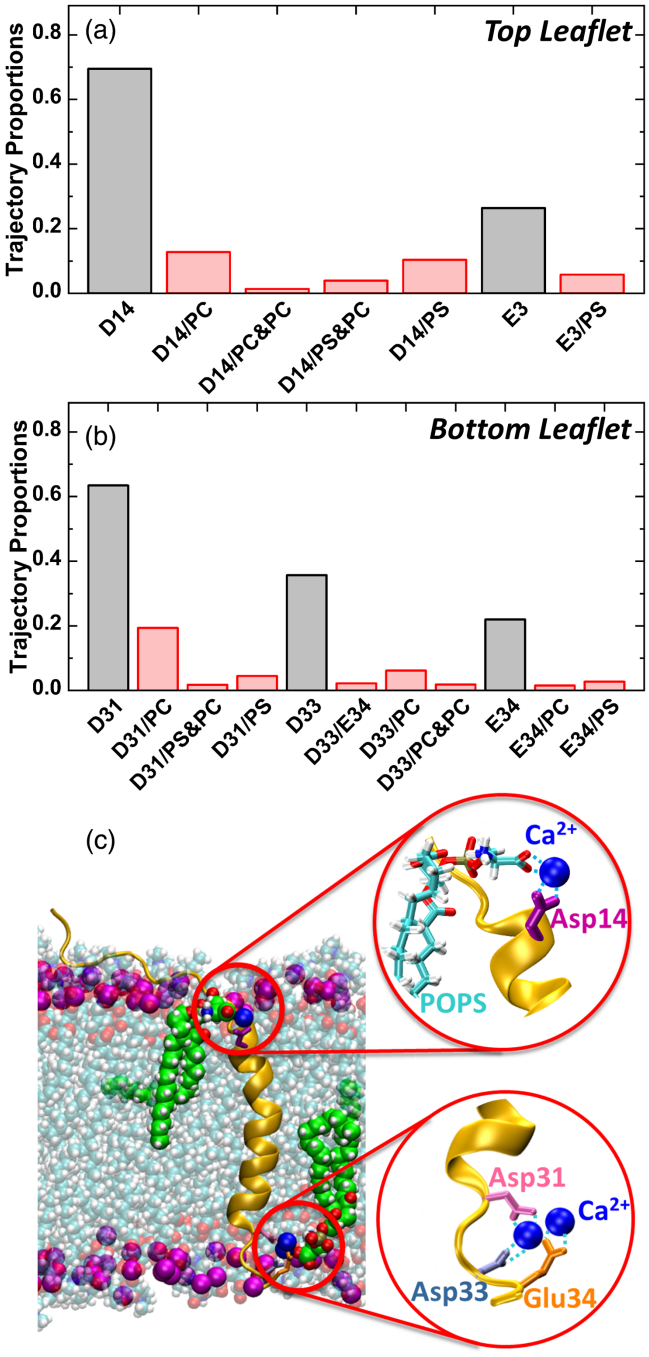

FIGURE 4 Ca^{2+}-mediated coordination of pH-low insertion peptide (pHLIP) and lipids. (a and b) Frequency of pHLIP acidic residue sidechains (gray bars) and both acidic residue sidechains and lipid polar moieties (red bars) in the first coordination shell of Ca^{2+} ions. Ca^{2+}-mediated pHLIP-lipid interactions between anionic residues and a single lipid are denoted as a.a./lipid, while simultaneous interactions with two lipids are indicated as: a.a./lipid&lipid. PC, phosphatidylcholine; PS, phosphatidylserine. (c) Simulation snapshot depicting the Ca^{2+}-mediated coordination of acidic residues in pHLIP and lipid polar moieties.

pHLIP, we measured the quenching efficiency by Br-containing lipids of two single-Trp pHLIP variants (pHLIP-W15 and pHLIP-V30W), in which native Trp were substituted for Phe. Unlike pHLIP-W15, in which the Trp resides in the cis-leaflet of the bilayer in the transmembrane form of pHLIP, V30W is instead expected to reside in the trans-leaflet. The efficiency of its depth-dependent Trp quenching by Br-containing lipids should, therefore, increase if PS is depleted in the trans-leaflet (due to the influx of Br-quenching PC lipids).

In the DA analysis, this increase in quenching efficiency would be reflected by an increase in the area (S) of the fitted data. In the case of W15, residing in the cis-leaflet, both the pH and Ca^{2+}-induced transmembrane forms of pHLIP-W15 yielded similar overall quenching parameters of $S = 14$ (Table 1). This is consistent with a similar PC:PS distribution in this cis-leaflet observed by MD for both insertion modes (Figure 5c,e). A similar quenching efficiency of $S = 15$ was also observed for trans-leaflet-residing V30W, but only in the case of Ca^{2+}-induced pHLIP insertion (Table 1). In contrast, the quenching efficiency of the V30W in pH-inserted pHLIP is increased to $S = 37$ (Table 1). This large increase in quenching can be explained only by a preferred location of quenching lipid species (brominated PC) in the peptide's vicinity in this leaflet. This is consistent with a substantial depletion of PS (and hence, increase in PC), observed in MD simulations for this case (Figure 5d).

3 | DISCUSSION

The cancer-targeting peptide pHLIP is a promising tool, capable of highly selective delivery of a variety of compounds to cancerous tissues.[17,45–48] The traditional model of pHLIP targeting and insertion relies solely on the mildly acidic extracellular environment generated by tumors.[5,37,49,50] Indeed, the ability of the peptide to insert into model membranes at acidic pH was demonstrated over two decades ago.[51] Our results, however, have shown that the targeting of pHLIP is a more complex process that relies on the coupling between pH, membrane lipid composition, and extracellular divalent cations (Figures 1 and 2a).[17]

The anionic lipid PS is a prominent modulator of pHLIP membrane interactions.[17,23,25] In the plasma membrane of healthy cells, PS is kept on the inner leaflet and is only transferred to the outer leaflet in diseased cells, such as apoptotic or cancerous cells.[11–13,30] The exposure of PS imparts an anionic character to the outside of cancer cells that differentiates them from healthy cells and influences protein/membrane interactions. This effect is demonstrated by our cellular data, which recapitulate the low targeting of "healthier tissues" (pH 7.4 and low PS) and high targeting of "cancerous tissues" (pH 7.0 and high PS) (Figure 1) observed in animal models.[6,47,52]

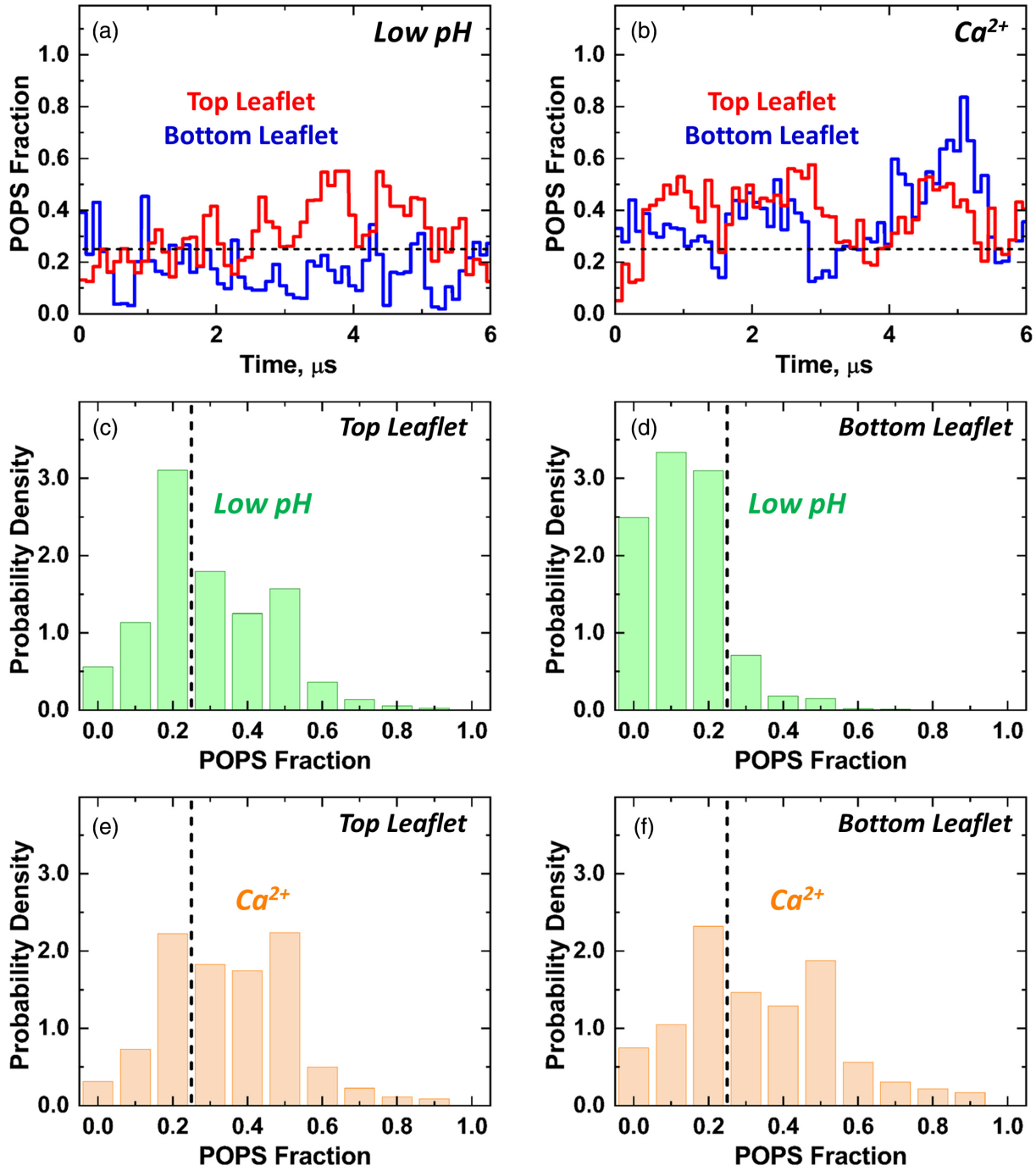

FIGURE 5 Effects of Ca^{2+} and low pH on lipid distribution near pH-low insertion peptide (pHLIP). (a and b) The phosphatidylserine (POPS) fraction within 15-Å of transmembrane pHLIP as a function of time in the top (red) and bottom (blue) leaflets. (c–f) Corresponding POPS distributions at low pH (green) or in the presence of Ca^{2+} (orange). In all panels, the dashed lines indicate the nominal POPS fraction.

Moreover, the effect of PS on pHLIP cellular targeting (and delivery capabilities[17]) is significantly enhanced by the presence of physiological levels of divalent cations (Figure 1, red).

A series of spectroscopic and computational studies were carried out in the presence of Ca^{2+} or at low pH (approximated in the MD simulations by protonating all acidic residues) to study the interactions between pHLIP and PS. All experimental measurements were in good agreement with our MD simulations, for example, differences in tilt angle between both conditions tested (Figure 2), as well as the depths and distribution widths of W15 (Figure 5) measured spectroscopically were reproduced by MD simulations.

Together, these measurements show that the presence of Ca^{2+} is crucial to understanding pHLIP-membrane

TABLE 1 Distribution analysis of depth-dependent fluorescence quenching of two single-Trp pHLIP variants

Single-Trp pHLIP (bilayer location in transmembrane state)	pH-inserted pHLIP (pH 4; no Ca^{2+})			Calcium-inserted pHLIP (pH 8; 2 mM Ca^{2+})		
	h_m, Å	σ, Å	S	h_m, Å	σ, Å	S
W15 (cis-leaflet)	10.0 ± 1.2	5.3 ± 2.8	*14 ± 7*	9.1 ± 0.2	2.7 ± 0.2	*14 ± 0.3*
V30W (trans-leaflet)	10.1 ± 0.5	6.7 ± 1.0	***37 ± 4***	10.7 ± 1.4	4.6 ± 2.7	*15 ± 8*

Note: Fluorescence intensities were measured in LUV containing Br-PC lipids, with Br atoms attached at different positions along the acyl chain (see Methods). Distribution analysis was applied to determine the mean value of the distribution of transverse distances of the Trp from the bilayer center (h_m), the width of the quenching profile (σ), and the overall quenching efficiency (S). The latter parameter (highlighted in italic) reflects the relative proportion of quenching (PC) and non-quenching lipids (PS) in the vicinity of the fluorophore. A very large S value, reported for V30W in the pH-inserted sample (bold) is consistent with the trans-leaflet depletion of PS observed in MD simulations in Figure 5.

Abbreviations: MD, molecular dynamics; pHLIP, pH-low insertion peptide.

interactions in vivo as it introduces several effects to these processes. First, Ca^{2+} interacts with acidic residues in pHLIP (Figure 4, gray), likely neutralizing their charge and lowering their free energy penalty to reside in the bilayer. Second, the presence of Ca^{2+} facilitates interactions between lipids and unprotonated acidic residues in pHLIP (Figure 4, red). These pHLIP-Ca^{2+}-lipid interactions are likely key to the stability, as well as the proper tilt, of the unprotonated form of pHLIP in the bilayer and link lipid-specific properties to protein-membrane interactions. And finally, the pH-induced and Ca^{2+}-induced insertion of pHLIP affects the lipid distribution in the vicinity of the peptide, which is different in the two leaflets (Figure 5, Table 1). The latter could have implications on the cooperativity of membrane binding and insertion of pHLIP, particularly due to the redistribution of PS lipids in cancer cells[11–13,30] and the sensitivity of pHLIP to PS asymmetry.[25]

The most prominent difference in lipid distribution between the protonated and Ca^{2+} simulations was observed in the trans-leaflet (Figure 5d,f). Under cellular conditions, this leaflet corresponds to the cytosolic side of the plasma membrane, where [Ca^{2+}] levels are extremely low. In contrast, Mg^{2+} levels inside the cell are in the mM range. As we have demonstrated previously, Mg^{2+} has similar effects on pHLIP insertion as Ca^{2+}.[17] Thus, it is plausible that the divalent-cation effects reported here by our simulations and experiments with model systems will be performed by different cations physiologically. Specifically, one can expect Ca^{2+} to have a more prominent role extracellularly, while Mg^{2+} will be more important inside the cell. Our future computational and experimental studies will address the effects of asymmetric distributions of both lipids and cations on pHLIP insertion.

Most of all pHLIP-Ca^{2+} interactions involved D14 and D31 (Figure 4 and Figure S3). Both residues have been previously identified to be crucial to the insertion mechanism of pHLIP in the absence of divalent cations. D14, for example, is key to the protonation-dependent insertion of pHLIP and the stability of the transmembrane state,[36,53] while the protonation of D31 is key to the initial insertion steps[54,55] and transmembrane stability.[56] The critical role of D31 in Ca^{2+}-mediated interactions suggests a possible explanation for the improved tumor selectivity of the clinical variant of pHLIP, pHLIP-Var3,[57,58] where the lack of C-terminal acidic residues (D31, D33, and D34) would prevent the Ca^{2+}-dependent stabilization of its C-terminus in the bilayer at neutral pH, likely reducing its non-specific Ca^{2+}-driven insertion into healthy cells and resulting in a more reliant pH-dependent targeting of cancerous tissues.

Our results highlight the importance of divalent cations such as Ca^{2+} on the interactions, stability, and insertion of peptides into cellular membranes under physiological conditions and indicate that the accurate representation of protein-membrane interactions in vitro requires cellular levels of divalent cations. We hypothesize that the stabilizing role of acidic residues in the bilayer by divalent cations is a general mechanism that extends to other systems, facilitating the membrane interaction and insertion of peptides/proteins previously assumed to be unfavorable. For example, the apoptotic regulators Bcl-xL and BAX, once thought to require protein activators to transition to lipid membranes, were recently shown to insert into membranes and refold into their active conformations (from soluble states) without the need for canonical activators through a lipid-dependent process that requires cytosolic levels of divalent cations.[9]

4 | MATERIALS AND METHODS

4.1 | Materials

POPC (1-palmitoyl-2-oleoyl-sn-glycero-3-phosphocholine), POPS (1-palmitoyl-2-oleoyl-sn-glycero-3-phospho-L-serine)

and all brominated-PC lipids (16:0-18:0(4,5-dibromo) PC, 16:0-18:0 (6-7BR) PC, 16:0-18:0 (9-10BR) PC, and 16:0-18:0 (11-12BR) PC) were purchased from Avanti Polar Lipids (Alabaster, AL). AlexaFluor488-maleimide was from Invitrogen (Carlsbad, CA). Peptides and the fluorescently-labeled conjugate were synthesized, purified, identified, and quantified as previously described.[17]

pHLIP variants used: pHLIP (AAEQNPIYWARYADWLFTTPLLLLDLALLVDADEGT),
pHLIP-W15 (AAEQNPIYFARYADWLFTTPLLLLDLALLVDADEGT),
pHLIP-V30W (AAEQNPIYFARYADFLFTTPLLLLDLALLWDADEGT).

4.2 | Cell culture

Human embryonic kidney (HEK29) cells were cultured in Dulbecco's Modified Eagle's medium high glucose supplemented with 10% FBS, 100 units/ml penicillin, and 0.1 mg/ml streptomycin. Human prostate adenocarcinoma LNCap cells were cultured in Rosewell Park Memorial Institute (RPMI) 1,640 medium supplemented with 10% FBS, 100 units/ml penicillin, and 0.1 mg/ml streptomycin. All cells were cultured in a humidified atmosphere of 5% CO_2 at 37°C.

4.3 | Annexin V quantification

HEK293 and LNCap cells were labeled with AlexaFluor-488 Annexin V (Invitrogen) according to the manufacturer's protocol. Briefly, the cells were harvested and washed once with binding buffer (10 mM HEPES-KOH, 140 mM NaCl, 2.5 mM $CaCl_2$, pH 7.4). The cells were incubated with AlexaFluor-488 Annexin V in binding buffer for 15 min at room temperature, washed once with binding buffer, and kept at 4°C until analysis. The amount of bound AlexaFluor-488 Annexin V was analyzed using a BDFacs Canto II flow cytometer equipped with a 488 nm argon laser and a 530/30 bandpass filter. The data was analyzed using FACSDiva version 6.1.1 software. The fluorescence data are expressed as mean arbitrary fluorescence units and were gated to include all healthy mammalian cells.

4.4 | Cell binding experiments

HEK293 and LNCap cells were harvested and washed with PBS, pH 7.4. AlexaFluor488-pHLIP was solubilized in an appropriate volume of 10 mM HEPES, 19.5 mM NaCl, pH 7.4 so that upon a twofold dilution, and after pH adjustment, a treatment concentration of 500 nM was obtained. The cells were incubated with AlexaFluor488-pHLIP at two times the desired concentration for 5 min at 37°C. Immediately following the incubation, an equal volume of 10 mM HEPES, 19.5 mM NaCl, pH 7.4 containing either 0 or 3.6 mM calcium was added to bring the final calcium concentration to 0 or 1.8 mM and incubated for an additional 5 min at 37°C. Then, the pH was adjusted using a pre-established volume of 10 mM HEPES buffered with acetic acid, pH 4.0, 19.5 mM NaCl, with either 0 or 1.8 mM calcium, and incubated for 10 min at 37°C. The cells were then washed at the same pH and calcium concentration as the treatment and fixed with 4% paraformaldehyde for 10 min at 4°C. The cells were resuspended in PBS and analyzed by flow cytometry as detailed above. Fluorescence was normalized to that observed with HEK293 cells treated at pH 7.4 with 0 mM calcium.

4.5 | Large unilamellar vesicles

The appropriate volume of chloroform lipid stocks was dried using a nitrogen stream and placed under a high vacuum to dry overnight. The dried lipid films were resuspended to a final concentration of 20 mM in 20 mM HEPES buffer + 100 mM NaCl pH 8 and the LUV were prepared by extrusion using a Mini-Extruder (Avanti Polar Lipids, Alabaster, AL) with 0.1 μm nucleopore polycarbonate membranes (Whatman, Philadelphia, PA).[59] LUV used in depth-dependent quenching experiments contained 50% brominated lipids.

4.6 | Trp fluorescence spectra

Trp emission spectra were collected on a Fluorolog FL3C-2 Ultrafast steady-state fluorimeter (Jobin Yvon, Edison, NJ) equipped with double-grating excitation and emission monochromators. The experimental temperature was kept at 25°C using a Peltier device from Quantum Northwest (Spokane, WA). Measurements were performed on 2 × 10 cuvettes oriented perpendicular to the excitation beam and collected after 20 min incubations using samples containing 2 μM pHLIP and 1 mM LUV.

Samples were excited at 280 nm and Trp spectra were collected between 300 and 460 nm at 1 nm steps using slits of 2 and 4 nm on the excitation and emission monochromators, respectively. The presented spectra are the average of 3 collected scans. Positions of maximum were determined by fitting the spectra to the log-normal distribution.[60]

4.7 | Distribution analysis of depth-dependent quenching

Trp fluorescence quenching experiments were performed with the single-Trp pHLIP W15 variant using lipid-attached bromine atoms as the quenching moieties.[39] The change in fluorescence intensity measured with LUV containing brominated lipids located at carbons 4–5, 6–7, 9–10, or 11–12 in the acyl tails of PC lipids residing at known bilayer depths was compared to the unquenched sample $\{QP[h] = [F_0/F(h)] - 1\}$. The resulting QP was analyzed by DA[41] with the following formula which approximates the transverse quenching with a sum of two mirror-imaged gaussian functions, G(h):

$$QP(h) = G(h) + G(-h) = \frac{S}{\sigma\sqrt{2\pi}} \exp\left[-\frac{(h-h_m)^2}{2\sigma^2}\right] + \frac{S}{\sigma\sqrt{2\pi}} \exp\left[-\frac{(h+h_m)^2}{2\sigma^2}\right],$$

where, h_m is the most probable depth of the probe measured from the bilayer center, σ, is the dispersion of the transverse QP, and S corresponds to the overall quenching efficiency.

4.8 | Oriented circular dichroism

OCD measurements were performed using a JASCO-810 spectropolarimeter (JASCO, Easton, MD). Spectra were obtained by creating a stack of oriented multilayers on a quartz disc as previously described.[17,61] Briefly, 0.1 mM pHLIP and a 10 mM lipid mixture containing a 25:75 M ratio of POPS and POPC were co-dissolved in methanol (1:100 peptide to lipid ratio). The multilayer stack was created by placing 2.5 μl of the peptide/lipid mixture in the center of a 2.5 cm disc. The solvent was then air-dried to a 1 cm diameter and hydrated using warm air at ~100% relative humidity. A drop of either 5 mM HEPES buffer pH 4 or 5 mM HEPES buffer pH 8 + 2 mM Ca^{2+} was added in between each layer of the stack and completely dried before continuing with multilayer stacking. The disc containing the multilayer stack was mounted on a sealed tube with the sample side pointing inwards. An average of 50 scans was collected at eight different orientations at 45° intervals along the central axis. The collected spectra were averaged and the background signal (determined by collecting the spectra of a multilayer stack in the absence of pHLIP) was subtracted. The presented spectra have been normalized to the ellipticity of their respective minimum due to difficulties calculating the peptide concentration along the beam path of each stack.

4.9 | Simulation systems

An all-atom model of pHLIP (AAEQNPIYWARY ADWLFTTPLLLLDLALLVDADEGT) was generated using the Molefacture Protein Builder plugin in VMD.[62] Residues 14 through 30 were assembled as an α-helix (backbone torsion angles $\phi = -57°$, $\psi = -47°$). Residues 1 through 13, and 34 through 36 were assembled in an extended conformation (backbone torsion angles $\phi = -180°$, $\psi = 180°$), and residues 31 and 32 in a turn conformation (backbone torsion angles $\phi = -60°$, $\psi = 30°$). The presence of proline at position 20 introduces a kink in the peptide configuration characterized by an angle of 140° between the helical segments preceding and following P20. The model peptide was embedded in a lipid bilayer composed of 1-palmitoyl-2-oleoyl-*sn*-glycero-3- phosphocholine (POPC) and 1,2-palmitoyl-oleoyl-*sn*-glycero-3-phosphoserine (POPS) with a 3:1 POPC: POPS ratio in a transmembrane configuration, with the axis defined by the geometric centers of L21 and D31 parallel to the membrane normal.

Two simulation systems were set up with different solution environments: 0.1 M $CaCl_2$ and 0.1 M NaCl. The simulation system setup was performed using CHARMM-GUI.[62] The $CaCl_2$ simulation system consisted of one pHLIP peptide with D25 protonated, 82 POPC lipids, 28 POPS lipids, 8,557 waters, 30 Ca^{2+} ions, and 28 Cl^- ions, for a total of 40,838 atoms and an initial simulation cell size of 76.8 Å × 73.0 Å × 102.6 Å. The NaCl simulation system consisted of one pHLIP peptide with all acidic sidechains (E3, D14, D25, D31, D33, E34) protonated, 217 POPC lipids, 72 POPS lipids, 17,039 waters, 100 Na^+ ions, and 29 Cl^- ions, for a total of 90,037 atoms and an initial simulation cell size of 107.2 Å × 105.8 Å × 103.6 Å.

4.10 | MD simulations

The initial equilibration of the simulation systems was performed on a conventional high-performance computing cluster using NAMD 2.11.[63] Each system was subjected to 20,000–30,000 steps of conjugate gradient energy minimization followed by a series of eight 80-ps runs at constant temperature (310 K) and pressure (1 atm) with harmonic restraints on the peptide-backbone atoms and the POPC carbonyl carbons with decreasing force constants equal to 10, 5, 2, 1, 0.5, 0.2, 0.1, and 0.05 kcal.mol^{-1}. Å^{-2}. Unrestrained dynamics

were then run for 5–10 ns. The CHARMM36m force field was used to model the peptide,[64] the CHARMM36 force field was used for lipids,[65,66] and ions were modeled with the NBFIX terms between Ca^{2+} ions and headgroup oxygens reported by Kim et al.[67] The TIP3P model was used for water.[68] The smooth particle-mesh Ewald summation method[69,70] was employed for the calculation of electrostatic interactions. Short-range real-space interactions were cut off at 12 Å, employing a force-based switching function. A reversible time step algorithm[71] was used to integrate the equations of motion with a time step of 1 fs. A Langevin scheme was used for temperature control and a Nosé–Hoover–Langevin piston[72,73] was used for pressure control.

4.11 | Microsecond-timescale simulations

After initial equilibration, both simulation systems were transferred to Anton2, a special-purpose supercomputer for biomolecular simulations, and run for 6 μs each.[74] The same force fields were used for the Anton2 simulations as the equilibration steps. The r-RESPA[75] algorithm was used to integrate the equations of motion with a time step of 7.5 fs for the long-range nonbonded forces and 2.5 fs for short-range nonbonded and bonded forces, and the k-Gaussian split Ewald[76] method was used for the long-range electrostatic interactions. The SHAKE[77] algorithm was employed to constrain hydrogen atom bond lengths. All simulations were performed at constant temperature (310 K) and pressure (1 atm) using Nosé-Hoover chains[78] and the Martyna-Tobias-Klein barostat.[72] The RESPA algorithm, temperature control, and pressure control were implemented using the multigrator Scheme.[79]

4.12 | Trajectory analysis

All the DAs were performed on the equilibrated portion of the trajectories, which ranged from 1 to 6 μs. The peptide helical axis was defined as the vector connecting the center of mass of pHLIP residues 29 to 31 to the center of mass of residues 21 to 23. The Ca^{2+} coordination shells were defined by the radial distribution function and the center-of-mass of each peptide or lipid moiety. Analyses were performed with VMD[62] and custom python scripts. Molecular graphics were generated with VMD.

AUTHOR CONTRIBUTIONS

Victor Vasquez-Montes: Investigation (equal); writing – original draft (equal); writing – review and editing (equal). **Vivek Tyagi:** Investigation (equal); writing – original draft (equal); writing – review and editing (equal). **Eden Sikorski:** Investigation (equal); writing – original draft (equal); writing – review and editing (equal). **Alexander Kyrychenko:** Investigation (equal); supervision (equal); writing – original draft (equal); writing – review and editing (equal). **J. Alfredo Freites:** Methodology (equal); supervision (equal); writing – original draft (equal); writing – review and editing (equal). **Alexey S. Ladokhin:** Methodology (equal); supervision (equal); writing – original draft (equal); writing – review and editing (equal). **Douglas J. Tobias:** Methodology (equal); supervision (equal); writing – original draft (equal); writing – review and editing (equal). **Damien Thévenin:** Methodology (equal); supervision (equal); writing – original draft (equal); writing – review and editing (equal).

ACKNOWLEDGMENTS

This work was supported by the National Institutes of Health (R01 GM126778). Victor Vasquez-Montes was supported in part by a BRTP fellowship from KUMC. Anton 2 computer time was provided by the Pittsburgh Supercomputing Center through the R01 GM116961 grant from the National Institutes of Health.

CONFLICT OF INTEREST

The authors have no conflict of interest to declare.

ORCID

Victor Vasquez-Montes https://orcid.org/0000-0001-7593-7293

REFERENCES

1. Dal Peraro M, van der Goot FG. Pore-forming toxins: Ancient, but never really out of fashion. Nat Rev Microbiol. 2016;14:77–92.
2. London E. How bacterial protein toxins enter cells; the role of partial unfolding in membrane translocation. Mol Microbiol. 1992;6:3277–3282.
3. White JM, Whittaker GR. Fusion of enveloped viruses in endosomes. Traffic. 2016;17:593–614.
4. Zasloff M. Antimicrobial peptides of multicellular organisms. Nature. 2002;415:389–395.
5. Reshetnyak YK, Segala M, Andreev OA, Engelman DM. A monomeric membrane peptide that lives in three worlds: In solution, attached to, and inserted across lipid bilayers. Biophys J. 2007;93:2363–2372.
6. Reshetnyak YK, Moshnikova A, Andreev OA, Engelman DM. Targeting acidic diseased tissues by pH-triggered membrane-associated peptide folding. Front Bioeng Biotechnol. 2020;8:335.
7. Weerakkody D, Moshnikova A, Thakur MS, et al. Family of pH (low) insertion peptides for tumor targeting. Proc Natl Acad Sci USA. 2013;110:5834–5839.

8. Strasser A, Cory S, Adams JM. Deciphering the rules of programmed cell death to improve therapy of cancer and other diseases. EMBO J. 2011;30:3667–3683.
9. Vasquez-Montes V, Rodnin MV, Kyrychenko A, Ladokhin AS. Lipids modulate the BH3-independent membrane targeting and activation of BAX and Bcl-xL. Proc Natl Acad Sci USA. 2021;118:e2025834118.
10. Chimento A, Casaburi I, Avena P, et al. Cholesterol and its metabolites in tumor growth: Therapeutic potential of statins in cancer treatment. Front Endocrinol (Lausanne). 2018;9:807.
11. Riedl S, Rinner B, Asslaber M, et al. In search of a novel target - phosphatidylserine exposed by non-apoptotic tumor cells and metastases of malignancies with poor treatment efficacy. Biochim Biophys Acta. 2011;1808:2638–2645.
12. Utsugi T, Schroit AJ, Connor J, Bucana CD, Fidler IJ. Elevated expression of phosphatidylserine in the outer membrane leaflet of human tumor cells and recognition by activated human blood monocytes. Cancer Res. 1991;51:3062–3066.
13. Zwaal RF, Comfurius P, Bevers EM. Surface exposure of phosphatidylserine in pathological cells. Cell Mol Life Sci. 2005;62:971–988.
14. Stelling MP, Motta JM, Mashid M, Johnson WE, Pavão MS, Farrell NP. Metal ions and the extracellular matrix in tumor migration. FEBS J. 2019;286:2950–2964.
15. Digiesi V, Bandinelli R, Bisceglie P, Santoro E. Magnesium in tumoral tissues, in the muscle and serum of subjects suffering from neoplasia. Biochem Med. 1983;29:360–363.
16. Wolf FI, Maier JAM, Nasulewicz A, et al. Magnesium and neoplasia: From carcinogenesis to tumor growth and progression or treatment. Arch Biochem Biophys. 2007;458:24–32.
17. Vasquez-Montes V, Gerhart J, Thevenin D, Ladokhin AS. Divalent cations and lipid composition modulate membrane insertion and cancer-targeting action of pHLIP. J Mol Biol. 2019;431:5004–5018.
18. Andreev OA, Engelman DM, Reshetnyak YK. Targeting diseased tissues by pHLIP insertion at low cell surface pH. Front Physiol. 2014;5:97.
19. Anemone A, Consolino L, Conti L, et al. Tumour acidosis evaluated in vivo by MRI-CEST pH imaging reveals breast cancer metastatic potential. Br J Cancer. 2021;124:207–216.
20. Vander Linden C, Corbet C. Therapeutic targeting of cancer stem cells: Integrating and exploiting the acidic niche. Front Oncologia. 2019;9:159.
21. Hashim AI, Zhang X, Wojtkowiak JW, Martinez GV, Gillies RJ. Imaging pH and metastasis. NMR Biomed. 2011;24:582–591.
22. Damaghi M, Wojtkowiak JW, Gillies RJ. pH sensing and regulation in cancer. Front Physiol. 2013;4:370.
23. Vasquez-Montes V, Gerhart J, King KE, Thevenin D, Ladokhin AS. Comparison of lipid-dependent bilayer insertion of pHLIP and its P20G variant. Biochim Biophys Acta Biomembr. 2018;1860:534–543.
24. Kyrychenko A, Vasquez-Montes V, Ulmschneider MB, Ladokhin AS. Lipid headgroups modulate membrane insertion of pHLIP peptide. Biophys J. 2015;108:791–794.
25. Scott HL, Heberle FA, Katsaras J, Barrera FN. Phosphatidylserine asymmetry promotes the membrane insertion of a transmembrane helix. Biophys J. 2019;116:1495–1506.
26. Barrera FN, Fendos J, Engelman DM. Membrane physical properties influence transmembrane helix formation. Proc Natl Acad Sci USA. 2012;109:14422–14427.
27. Connor J, Bucana C, Fidler IJ, Schroit AJ. Differentiation-dependent expression of phosphatidylserine in mammalian plasma membranes: Quantitative assessment of outer-leaflet lipid by prothrombinase complex formation. Proc Natl Acad Sci USA. 1989;86:3184–3188.
28. Rao LV, Tait JF, Hoang AD. Binding of annexin V to a human ovarian carcinoma cell line (OC-2008). Contrasting effects on cell surface factor VIIa/tissue factor activity and prothrombinase activity. Thromb Res. 1992;67:517–531.
29. Schroder-Borm H, Bakalova R, Andra J. The NK-lysin derived peptide NK-2 preferentially kills cancer cells with increased surface levels of negatively charged phosphatidylserine. FEBS Lett. 2005;579:6128–6134.
30. Tan LT, Chan K-G, Pusparajah P, et al. Targeting membrane lipid a potential cancer cure? Front Pharmacol. 2017;8:12.
31. Vallabhapurapu SD, Blanco VM, Sulaiman MK, et al. Variation in human cancer cell external phosphatidylserine is regulated by flippase activity and intracellular calcium. Oncotarget. 2015;6:34375–34388.
32. Slaybaugh G, Weerakkody D, Engelman DM, Andreev OA, Reshetnyak YK. Kinetics of pHLIP peptide insertion into and exit from a membrane. Proc Natl Acad Sci USA. 2020;117:12095–12100.
33. Burck J, Wadhwani P, Fanghanel S, Ulrich AS. Oriented circular dichroism: A method to characterize membrane-active peptides in oriented lipid bilayers. Acc Chem Res. 2016;49:184–192.
34. Wu Y, Huang HW, Olah GA. Method of oriented circular dichroism. Biophys J. 1990;57:797–806.
35. Vila-Vicosa D, Silva TFD, Slaybaugh G, Reshetnyak YK, Andreev OA, Machuqueiro M. Membrane-induced p K_a shifts in wt-pHLIP and its L16H variant. J Chem Theory Comput. 2018;14:3289–3297.
36. Musial-Siwek M, Karabadzhak A, Andreev OA, Reshetnyak YK, Engelman DM. Tuning the insertion properties of pHLIP. Biochim Biophys Acta. 2010;1798:1041–1046.
37. Andreev OA, Karabadzhak AG, Weerakkody D, Andreev GO, Engelman DM, Reshetnyak YK. pH (low) insertion peptide (pHLIP) inserts across a lipid bilayer as a helix and exits by a different path. Proc Natl Acad Sci USA. 2010;107:4081–4086.
38. Shu NS, Chung MS, Yao L, An M, Qiang W. Residue-specific structures and membrane locations of pH-low insertion peptide by solid-state nuclear magnetic resonance. Nat Commun. 2015;6:7787.
39. Ladokhin AS. Analysis of protein and peptide penetration into membranes by depth-dependent fluorescence quenching: Theoretical considerations. Biophys J. 1999;76:946–955.
40. Ladokhin AS. Distribution analysis of depth-dependent fluorescence quenching in membranes: A practical guide. Methods Enzymol. 1997;278:462–473.
41. Ladokhin AS. Measuring membrane penetration with depth-dependent fluorescence quenching: Distribution analysis is coming of age. Biochim Biophys Acta. 2014;1838:2289–2295.
42. Ladokhin AS, Kyrychenko A, Rodnin MV, Vasquez-Montes V. Conformational switching, refolding and membrane insertion

of the diphtheria toxin translocation domain. Methods Enzymol. 2021;649:341–370.
43. Karabadzhak AG, Weerakkody D, Wijesinghe D, et al. Modulation of the pHLIP transmembrane helix insertion pathway. Biophys J. 2012;102:1846–1855.
44. Melcrova A, Pokorna S, Pullanchery S, et al. The complex nature of calcium cation interactions with phospholipid bilayers. Sci Rep. 2016;6:38035.
45. Svoronos AA, Bahal R, Pereira MC, et al. Tumor-targeted, cytoplasmic delivery of large, polar molecules using a pH-low insertion peptide. Mol Pharm. 2020;17:461–471.
46. Zhao Z, Li C, Song B, et al. pH low insertion peptide mediated cell division cycle-associated protein 1 -siRNA transportation for prostatic cancer therapy targeted to the tumor microenvironment. Biochem Biophys Res Commun. 2018;503:1761–1767.
47. Cheng CJ, Bahal R, Babar IA, et al. MicroRNA silencing for cancer therapy targeted to the tumour microenvironment. Nature. 2015;518:107–110.
48. Wyatt LC, Moshnikova A, Crawford T, Engelman DM, Andreev OA, Reshetnyak YK. Peptides of pHLIP family for targeted intracellular and extracellular delivery of cargo molecules to tumors. Proc Natl Acad Sci USA. 2018;115:E2811–E2818.
49. Reshetnyak YK, Andreev OA, Lehnert U, Engelman DM. Translocation of molecules into cells by pH-dependent insertion of a transmembrane helix. Proc Natl Acad Sci USA. 2006;103:6460–6465.
50. Reshetnyak YK, Andreev OA, Segala M, Markin VS, Engelman DM. Energetics of peptide (pHLIP) binding to and folding across a lipid bilayer membrane. Proc Natl Acad Sci USA. 2008;105:15340–15345.
51. Hunt JF, Rath P, Rothschild KJ, Engelman DM. Spontaneous, pH-dependent membrane insertion of a transbilayer α-helix. Biochemistry. 1997;36:15177–15192.
52. Andreev OA, Dupuy AD, Segala M, et al. Mechanism and uses of a membrane peptide that targets tumors and other acidic tissues in vivo. Proc Natl Acad Sci USA. 2007;104:7893–7898.
53. Fendos J, Barrera FN, Engelman DM. Aspartate embedding depth affects pHLIP's insertion pKa. Biochemistry. 2013;52:4595–4604.
54. Otieno SA, Hanz SZ, Chakravorty B, et al. pH-dependent thermodynamic intermediates of pHLIP membrane insertion determined by solid-state NMR spectroscopy. Proc Natl Acad Sci USA. 2018;115:12194–12199.
55. Hanz SZ, Shu NS, Qian J, et al. Protonation-driven membrane insertion of a pH-low insertion peptide. Angew Chem Int Ed Engl. 2016;55:12376–12381.
56. Burns V, Mertz B. Using simulation to understand the role of titration on the stability of a peptide-lipid bilayer complex. Langmuir. 2020;36:12272–12280.
57. Crawford T, Moshnikova A, Roles S, et al. pHLIP ICG for delineation of tumors and blood flow during fluorescence-guided surgery. Sci Rep. 2020;10:18356.
58. Tapmeier TT, Moshnikova A, Beech J, et al. The pH low insertion peptide pHLIP variant 3 as a novel marker of acidic malignant lesions. Proc Natl Acad Sci USA. 2015;112:9710–9715.
59. Mayer LD, Hope MJ, Cullis PR. Vesicles of variable sizes produced by a rapid extrusion procedure. Biochim Biophys Acta. 1986;858:161–168.
60. Ladokhin AS, Jayasinghe S, White SH. How to measure and analyze tryptophan fluorescence in membranes properly, and why bother? Anal Biochem. 2000;285:235–245.
61. Wimley WC, White SH. Designing transmembrane alpha-helices that insert spontaneously. Biochemistry. 2000;39:4432–4442.
62. Humphrey W, Dalke A, Schulten K. VMD: Visual molecular dynamics. J Mol Graph. 1996;14:33–38.
63. Phillips JC, Braun R, Wang W, et al. Scalable molecular dynamics with NAMD. J Comput Chem. 2005;26:1781–1802.
64. Huang J, Rauscher S, Nawrocki G, et al. CHARMM36m: An improved force field for folded and intrinsically disordered proteins. Nat Methods. 2017;14:71–73.
65. Klauda JB, Venable RM, Freites JA, et al. Update of the CHARMM all-atom additive force field for lipids: Validation on six lipid types. J Phys Chem B. 2010;114:7830–7843.
66. Best RB, Zhu X, Shim J, et al. Optimization of the additive CHARMM all-atom protein force field targeting improved sampling of the backbone phi, psi and side-chain chi(1) and chi(2) dihedral angles. J Chem Theory Comput. 2012;8:3257–3273.
67. Kim S, Patel DS, Park S, Slusky J, Klauda, JB, Widmalm G, Im W. Bilayer properties of lipid a from various gram-negative bacteria. Biophys J. 2016;111:1750–1760.
68. Jorgensen WL, Chandrasekhar J, Madura JD, Impey RW, Klein ML. Comparison of simple potential functions for simulating liquid water. J Chem Phys. 1983;79:926–935.
69. Essmann U, Perera L, Berkowitz ML, Darden T, Lee H, Pedersen LG. A smooth particle mesh Ewald method. J Chem Phys. 1995;103:8577–8593.
70. Darden T, York D, Pedersen L. Particle mesh Ewald: An Nlog(N) method for Ewald sums in large systems. J Chem Phys. 1993;98:10089–10092.
71. Grubmüller H, Heller H, Windemuth A, Schulten K. Generalized Verlet algorithm for efficient molecular dynamics simulations with long-range interactions. Mol Simul. 1991;6:121–142.
72. Martyna GJ, Tobias DJ, Klein ML. Constant-pressure molecular-dynamics algorithms. J Chem Phys. 1994;101:4177–4189.
73. Feller SE, Zhang Y, Pastor RW, Brooks BR. Constant pressure molecular dynamics simulation: The Langevin piston method. J Chem Phys. 1995;103:4613–4621.
74. Shaw DE, Grossman JP, Bank JA, et al. Anton 2: Raising the bar for performance and programmability in a special-purpose molecular dynamics supercomputer. *SC14: International Conference for High Performance Computing, Networking, Storage and Analysis*. 2014:41–53.
75. Tuckerman M, Berne BJ. Reversible multiple time scale molecular dynamics. J Chem Phys. 1992;97:1990–2001.
76. Shan Y, Klepeis JL, Eastwood MP, Dror RO, Shaw DE. Gaussian split Ewald: A fast Ewald mesh method for molecular simulation. J Chem Phys. 2005;122:054101.
77. Ryckaert J-P, Ciccotti G, Berendsen HJC. Numerical integration of the Cartesian equations of motion of a system with constraints: Molecular dynamics of *n*-alkanes. J Comput Phys. 1977;23:327–341.
78. Martyna GJ, Klein ML, Tuckerman M. Nose-Hoover chains - the canonical ensemble via continuous dynamics. J Chem Phys. 1992;97:2635–2643.

79. Lippert RA, Predescu C, Ierardi DJ, et al. Accurate and efficient integration for molecular dynamics simulations at constant temperature and pressure. J Chem Phys. 2013;139:164106.

SUPPORTING INFORMATION

Additional supporting information can be found online in the Supporting Information section at the end of this article.

How to cite this article: Vasquez-Montes V, Tyagi V, Sikorski E, Kyrychenko A, Freites JA, Thévenin D, et al. Ca^{2+}-dependent interactions between lipids and the tumor-targeting peptide pHLIP. Protein Science. 2022;31(9):e4385. https://doi.org/10.1002/pro.4385